Alexandria Engineering Journal (2022) xxx, xxx–xxx

HOSTED BY

Alexandria University

Alexandria Engineering Journal

www.elsevier.com/locate/aej
www.sciencedirect.com

MHD natural convection of Fe_3O_4- MWCNT/ Water hybrid nanofluid filled in a porous annulus between a circular cylinder and Koch snowflake

Abed Mourad [a], Abderrahmane Aissa [a], Azher M. Abed [b], Davood Toghraie [c,*], Omid Ali Akbari [d], Kamel Guedri [e], Obai Younis [f], Riadh Marzouki [g]

[a] *(LPQ3M), University of Mascara, Algeria*
[b] *Air Conditioning and Refrigeration Techniques Engineering Department, Al-Mustaqbal University College, Iraq*
[c] *Department of Mechanical Engineering, Khomeinishahr Branch, Islamic Azad University, Khomeinishahr, Iran*
[d] *Young Researchers and Elite Club, Khomeinishahr Branch, Islamic Azad University, Khomeinishahr, Iran*
[e] *Department of Mechanical Engineering, College of Engineering in Wadi Addwasir, Prince Sattam Bin Abdulaziz University, Saudi Arabia*
[f] *Department Mechanical Engineering, College of Engineering at Wadi Addwaser Prince Sattam Bin Abdulaziz University, Wadi Addwaser, Saudi Arabia*
[g] *Chemistry Department, College of Science, King Khalid University, P.O. Box 394, Abha 61413, Saudi Arabia*

Received 27 February 2022; revised 11 July 2022; accepted 16 September 2022

KEYWORDS

Magneto-hydrodynamic;
Natural convection;
Koch snowflake;
Hybrid nanofluid;
Porous media Galerkin finite element technique

Abstract In this work, the numerical investigation was conducted for the MHD natural convection and entropy generation characteristics of water-based hybrid nanofluid (Fe_3O_4-MWCNT) in a porous annulus between a cooled circular cylinder and a heated Koch snowflake subjected to a uniform magnetic force. The novelty of this work is presented by the special shape and different studied positions of the hot barrier. The governing equations are explained by employing the Finite Element Method. The impacts of nanoparticle volume fraction (φ = 2 %, 3%,4%, and 5 %), Rayleigh number (Ra = 10^3 to 10^6), Hartman number (Ha = 0,25,50,100), Darcy number (Da = 10^{-2}, 10^{-3}, 10^{-4}, and 10^{-5}), and the position of the Koch snowflake (four cases) on the distributions of isotherms, streamlines, average Nusselt number (Nu_{avg}) as well as on total entropy generation and Bejan number are thoroughly examined. The computational outcomes indicate that increasing the Ra number is possible by changing the temperature between the hot and cold sources. By increasing this parameter, the buoyancy force of the fluid is strengthened. As the Da number increases, the penetration of the flow cross-section in the cavity increases, and the flow circulates in the cavity with less depreciation due to the buoyancy force. Applying Lorentz force, if not in the direction of natural flow, causes the flow velocity to be depleted and fluid flow in the cavity

* Corresponding author.
E-mail addresses: davoodtoghraie@iaukhsh.ac.ir, Toghraee@iaukhsh.ac.ir (D. Toghraie).
Peer review under responsibility of Faculty of Engineering, Alexandria University.

https://doi.org/10.1016/j.aej.2022.09.035

Please cite this article in press as: A. Mourad et al., MHD natural convection of Fe_3O_4- MWCNT/Water hybrid nanofluid filled in a porous annulus between a circular cylinder and Koch snowflake$3O_4$- MWCNT/Water hybrid nanofluid filled –>, Alexandria Eng. J. (2022), https://doi.org/10.1016/j.aej.2022.09.035

Nomenclature

Cp	Heat capacitance (J kg^{-1} K^{-1})
g	Gravity (m/s^{-2})
Ha	Hartmann number
Nu	Nusselt number
p	Pressure (Nm^{-2})
P	Dimensionless pressure
Pr	Prandtl number
R	Base circular radius of the block (m)
Ra	Rayleigh number
T	Dimension temperature (K)
u, v	Dimensional velocity components along x and y directions (m/s)
U, V	Non-dimensional velocity components along with x and y directions
x, y	Cartesian coordinates (m)
X, Y	Non-dimensional coordinates

Greek symbols

A	Thermal diffusivity (m^2/s)
β	Thermal expansion coefficient (K^{-1})
k	Thermal conductivity (W $m^{-1}K^{-1}$)
μ	Dynamic viscosity, kg m^{-1} s
υ	Kinematic viscosity (m^2/s)
ρ	Density (kg m^{-3})
ϕ	Volume fraction of the nanoparticles
θ	Non-dimensional temperature

Subscripts

C	Cold
h	Hot
F	Fluid
P	Solid particles
S	Solid block
Avg	Average

to be facilitated. With increasing Ra number, the application of Lorentz force with different intensities becomes important due to the importance of fluid circulation in the cavity. Applying a Lorentz force with a higher Ha number at high Ra numbers reduces heat transfer due to junction balance and flow separation on hot and cold surfaces. In the lower Ra numbers, the Bejan number tends to 1, indicating a significant increase in the temperature gradient in the cavity and the expansion of the thermal boundary layer at low fluid velocities. At the highest Ra, increasing Ha from 0 to 100 decreases Nu_{avg} by 50 %, while decreasing Da from 10^{-2} to 10^{-5} reduces Nu_{avg} by 70 %.

1. Introduction

Choi [1] pioneered the concept of nanofluids, which are the dispersion of nanoparticles with a diameter of 1–100 nm into thermal working fluids to boost their thermal conductivity. Several researchers have recently conducted on heat transfer, fluid flow, mass transfer in a varied range of applications, comprising cooling of electronics and engines, heat exchangers, energy storage, solar collectors, machining technology, photovoltaic cells thermal management, petroleum industries, lubricants, and drug delivery [2–11]. Consequently, researchers made a substantial effort to develop the heat transfer ability of nanofluids through theoretical and experimental investigations [12–16]. Fins are an excellent solution for boosting heat transfer to liquids, which explains why they are present in a broad variety of applications, including heat exchangers, thermal storage systems and electronics cooling. Thus, developing fins to promote nanofluids' free convection gained greater attention from scientists in the previous decades. Aly et al. [17] explored the influence of a magnetic force on convection within a finned chamber loaded with a nanofluid. The results indicate that the presence of four fins is an excellent tool for cooling a nanofluid contained inside a cavity. The rotation of an implanted rectangle has a substantial effect on the nanofluid motions and flow characteristics. Massoudi et al. [18] examined the influence of a magnetic force and radiation on the heat transfer of nanofluid contained in a *T*-shaped cavity equipped with trapezoidal fins. The noteworthy results indicate that raising the Rayleigh number, the radiation parameter, and the trapezoidal fins' height enhances convection. Hussain et al. [19] researched the effect of fins and magnetic fields on heat transfer within lid-driven cavities loaded with Cu/water nanofluid. It is concluded that the existence of fins substantially influences fluid motion and heat transfer when compared to the finless chamber. Zhang et al. [20] examined the influence of the temperature on the dynamic behaviors of magnetorheological gel. Gireesha et al. [21] explained the convection of a hybrid nanofluid (Ag-MgO/Water) near a permeable fin moving horizontally with constant velocity and in the presence of heat radiation. The obtained results demonstrate that a fin with a known convective coefficient at the tip exhibits a higher heat transfer rate than a fin with an insulated tip. Hejri et al. [22] conducted a computational analysis utilizing The Koo-Kleinstreuer-Li (KKL) model to characterize all elements of convective flow and determine the optimal design for a heat sink loaded with copper oxide/water nanofluid. The findings confirm that narrower fins result in a more effective heat dissipation mechanism. Gholami et al. [23] examined the effect of introducing dimpled fins to a vertical channel wall carrying a variety of water-based nanofluids (Al_2O_3, TiO_2, Cu, and car-

bon nanotubes). Sheremet et al. [24] discussed the influence of sinusoidal-heated sidewalls and porous insertion on the free convection of various nanofluids in a square space. The findings demonstrate that the vertical orientation and penetration of the interior porous block might be beneficial features for enhancing heat transfer. Yan et al. [25] researched the influence of nanoparticle morphology on the natural convection and entropy generation of nanofluid when it was filled into a square container outfitted with fins of various shapes and exposed to magnetic forces. By employing two-phase model linked with Darcy–Brinkman–Forchheimer model, Siavashi et al. [26] provided a numerical investigation of free convection and entropy generation in a squared chamber saturated with Cu/water nanofluid and equipped with two porous fins. Outputs reveal that the addition of permeable fins with a high Da number boosts heat transfer whereas fins with a low Da number may hinder the convection and drop the Nusselt number. Al-Farhany et al. [27] studied the influence of fins on MHD natural convection in a permeable inclined enclosure loaded with ferrofluid and heated differentially. The findings indicate that raising the modified Ra number, fins length, and Da number enhances the average Nusselt number, but increasing the Ha number reduces it. Regarding these cavities with an embedded obstacle, free convection in a wavy walled chamber with a heated cylinder was examined by Abdulkadhim et al. [28] and in another study, Abdulkadhim et al. [29] examined the natural convection of nanofluid in I shaped wavy walled enclosure partitioned into two layers and infiltrated with multi-pipes of heat exchangers. Numerous studies were conducted on the free convection of water-based nanofluids in annulus-type enclosures with varying geometric configurations and external conditions. For example, in the circular annulus, Seyyedi et al. [30] determined that increasing the outer to the inner radius ratio improves the Nu_{avg}. Tayebi et al. [31] reported that by incorporating a solid conductive partition into the annulus shape. They could significantly alter the nanofluid's natural convection characteristics and temperature distributions. Hu et al. [32] revealed that while the volume fraction and radius ratio substantially impact flow and thermal fields, the nanoparticle diameter has a negligible effect. The impact of the vertical and horizontal eccentricity of the inner heated cylinder was investigated by Gholamalipour et al. [33]. They observed that the downward eccentric annulus exhibits optimal heat transfer and entropy generation performance. Belabid et al. [34] noted that the wall waviness in an annulus with circular-sinusoidal cylinders impacted the thermo-bioconvective instabilities and the flow pattern. As for half-annulus enclosures, Oğlakkaya et al. [35] explored the influence of tilting the enclosure or the magnetic field on the nanofluid's free convection. They determined that the enclosure's inclination angle may be employed as a controlling factor to optimize heat transfer through convection and flow. Guan et al. [36] investigated the chemical environment and magnetic moment effects on point defect formations in CoCrNi-based concentrated solid-solution alloys. Motlagh et al. [37] reserached the natural convection of nanofluid inside a tilted permeable half-annulus enclosure by employing Buongiorno and Darcy models. They reported that growing the enclosure's inclination angle reduces the heat transfer rate at high porosity and Ra numbers. Hatami et al. [38] examined the impact of variable magnetic field on the heat transfer of a semi-annulus enclosure filled by Fe_3O_4/water nanofluid. According to their findings, raising the Ha number creates a drop on the Nusselt number. Other studies of a similar kind are available in the literature. Munawar et al. [39] researched the entropy generation and the MHD free convection of a hybrid nanofluid in a corrugated triangular annulus furnished with a central triangular heater. Miles et al. [40] examined free convection and the generation of entropy in a vertical porous annulus loaded with nanofluids. They found that the incorporation of nanoparticles enhances heat transfer and total entropy generation. Dogonchi et al. [41] researched the impact of a uniform magnetic field and thermal radiation on thermo-hydrodynamics of nanofluid in a wavy circular cylinder with an inner heated rhombus object. Bouzerzour et al. [42] explored the free convection of a Cu/water nanofluid within a partly heated annulus formed by two elliptical cylinders. The findings indicated that heat transfer might be improved by raising the Ra number or the volume percentage of nanoparticles and positioning the heaters on both sides of the inner cylinder wall. Similarly, Sheikholeslami et al. [43] explored the influence of Lorentz forces on the flow and heat transfer of a water/Al_2O_3 nanofluid inside an enclosure made up of a cold square cylinder and a heated horizontal elliptic cylinder. Berrahil et al. [44] reserached the MHD free convection of water-based Al_2O_3 nanofluid within a differentially heated vertical annulus. They shows that the magnetic field has a stronger influence in the radial direction. Aboud et al. [45] examined the MHD mixed convection of a Newtonian Cu/water nanofluid within a circular annulus container with an exterior spinning cylinder. They reported that the stream function grows as the power-law index rises. The average Nusselt number rises as the Richardson number decreases, since forced convection improves heat transfer. Tayebi et al. [46] researched the MHD natural convection and entropy genaration of a nanofluid contained between two circular cylinders with inner heated cylinder equipped with rectangular fins of various lengths. According to their findings, irreversibility due to thermodynamic effects dominates inside the annulus for low Ra numbers, and with increasing Ra number, it ceases to be the primary contributor to total entropy generation. Shahsavar et al. [47] explained the entropy generation and convection flow of a biological nanofluid in a horizontal annulus with embedded fins. The simulation results suggest that attaching fins and increasing their number greatly increases the entropy generation due to heat transfer by up to 39.07 % and increases Nu by up to 35.50 %, respectively, as compared to a finless annulus. The purpose of this study is to look into the impact of temporary changes in barrier, application of magnetic force of different intensities, increase of Ra and Da numbers on natural convection of porous annulus cavity between circular cylinder and Koch snowflake.

According to the previous literature review and the extent of the author's knowledge, no research models the convective heat transfer of a hybrid nanofluid loaded in a permeable annulus between a circular cylinder and a Koch snowflake. Thus, the primary goal of this work is to fill that gap by analyzing natural convection within an enclosure between a cold circular cylinder and a hot Koch snowflake packed with porous media and saturated with Fe_3O_4-MWCNT/Water nanofluid. The study employs a two-dimensional single-phase, Newtonian nanofluid model to explore the impact of domain porosity, magnetic field, and the eccentricity of the inner Koch snowflake. As a result, we believe the present work is unique

and useful. The Finite Element Method was used to make numerical calculations (FEM). The flow visualization results are shown as isotropic lines, isotherms, and streamlines contours for various Hartmann numbers, Darcy numbers, and eccentricity parameters. Additionally, the average Nusselt numbers for the hot walls and the Bejan number are calculated and examined numerically.

2. Physical model description

Fig. 1 depicts the study's conceptual framework. The figure shows an outside circular cylinder maintained at a low temperature (T_c) and an inner Koch snowflake maintained at a high temperature (T_h). A Newtonian hybrid nanofluid is used to fill the porous area between the two walls. Fe3O4 and MWCNT nanoparticles were used in this investigation, and their respective thermophysical solid and liquid characteristics are reported in Table 1. Nanoparticles representing the solid phase and water representing the liquid phase are in thermal equilibrium, and water and nanoparticles have the same movement (i.e., same magnitude and flow direction). Numerous simplifying assumptions are used, including two-dimensional, incompressible, steady-state, and laminar motion.

3. Governing equations and boundary conditions

3.1. Governing equations

In this section, we analyze the steady-two-dimensional free convection of a hybrid nanofluid within a circular-shaped chamber with a diameter of L and a heated Koch snowflake-shaped hole in the enclosure's center, as seen in Fig. 1. The enclosure under investigation is loaded with permeable media and saturated with a hybrid nanofluid. Both the outside and interior boundaries are seen as impenetrable. The mixed liquid acts like a water-based hybrid (Fe_3O_4-MWCNT) nanofluid within the cavity. Brinkman's model [48] is used to represent a permeable media mathematically. Consider the Cartesian coordinates for the Navier-Stokes equations in light of the above assumptions, which may be shown in the dimensional model as follows [49–51]:

$$Continuity\ \frac{\partial(u)}{\partial x}+\frac{\partial(v)}{\partial y}=0 \tag{1}$$

$$\mathrm{X}-\mathrm{momentum}\quad u\frac{\partial u}{\partial x}+v\frac{\partial u}{\partial y} =-\frac{\partial p}{\partial x}+\frac{(\mu)}{(\rho)}\left(\frac{\partial^2 u}{\partial x^2}+\frac{\partial^2 u}{\partial y^2}\right)-\frac{(\mu)_{bf}}{(\rho)K}u \tag{2}$$

$$Y-momentum: u\frac{\partial v}{\partial x}+v\frac{\partial v}{\partial y} =-\frac{1}{(\rho)}\frac{\partial p}{\partial y}+\frac{(\mu)}{(\rho)}\left(\frac{\partial^2 v}{\partial x^2}+\frac{\partial^2 v}{\partial y^2}\right)+(\beta)g(T-T_c)-\frac{(\mu)}{(\rho)K}v-\frac{\sigma B_0^2}{(\rho)}v \tag{3}$$

$$Energy: u\frac{\partial T}{\partial x}+v\frac{\partial T}{\partial y}=\alpha\left[\left(\frac{\partial^2 T}{\partial x^2}+\frac{\partial^2 T}{\partial y^2}\right)\right] \tag{4}$$

To rebuild the equations in a dimensionless form, the following requirements have been considered:*Dimensionless scales*

$$X,Y=\frac{x,y}{L},\quad U,V=\frac{(u,v)L}{\alpha_{fl}},\quad \theta=\frac{T-T_c}{T_h-T_c}$$

Dimensionless numbers

$$P=\frac{(p+\rho g)L^2}{\rho\alpha_{fl}^2}$$

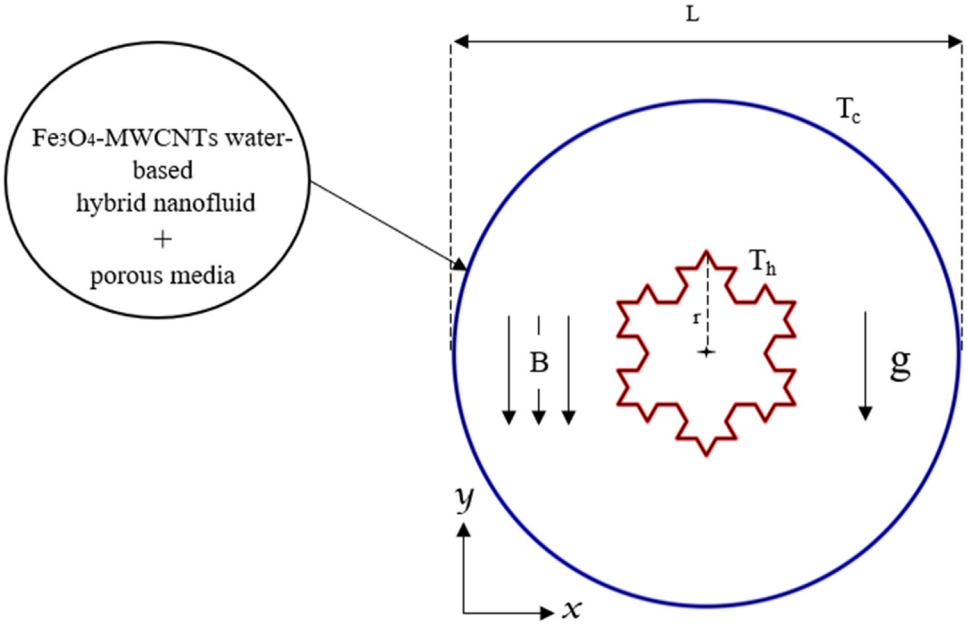

Fig. 1 The schematic of the present study.

Table 1 Thermophysical characteristics of (Fe_3O_4- MWCNT/ water (50–50%)) [54].

Properties	ρ(kg/m^3)	C_p (J/kg K)	k(W/m K)	σ(S/ m)	β (K $^{-1}$)
Water	997.1	4179	0.613	5.5×10^{-6}	21×10^{-5}
Fe_3O_4	5810	670	6	2.5×10^{-4}	1.3×10^{-5}
MWCNT	2100	711	3000	1.9×10^{-4}	4.2×10

$$Ra = \frac{g\beta_{fl}(T_h - T_c)L^3}{\alpha_{fl}\nu_{fl}} (Rayleigh\ number)$$

$$Da = \frac{\lambda}{L^2} (Darcy\ number)$$

$$\mathrm{Pr} = \frac{\nu_{fl}}{\alpha_{fl}} (Prandtl\ number)$$

The following parameters characterize the Fe_3O_4-MWCNT/water nanofluid [52]:

$$\rho_{nf} = (1-\phi)\rho_{fl} + \phi_s \tag{5}$$

$$(\rho c_p)_{nf} = (1-\phi)(\rho c_p)_{fl} + \phi(\rho c_p)_s \tag{6}$$

$$(\rho\beta)_{nf} = (1-\phi)\rho_{fl} + \phi(\rho\beta)_s \tag{7}$$

$$\frac{k_{nf}}{k_{fl}} = \frac{k_s + 2k_{fl} - 2\phi(k_{fl} - k_s)}{k_s + 2k_{fl} + 2\phi(k_{fl} - k_s)} \tag{8}$$

$$\mu_{nf} = \frac{\mu_{fl}}{(1-\phi)^{0.25}} \tag{9}$$

The characteristics of Fe_3O_4 and MWCNT nanoparticles are determined by [53].

$$\varphi_{np} = \varphi_{Fe_3O_4} + \varphi_{MWCNT} \tag{10}$$

$$\rho_{np} = \frac{\varphi_{Fe_3O_4}\rho_{Fe_3O_4} + \varphi_{MWCNT}\rho_{MWCNT}}{\varphi} \tag{11}$$

$$(c_p)_{np} = \frac{\varphi_{Fe_3O_4}(c_p)_{Fe_3O_4} + \varphi_{MWCNT}(c_p)_{MWCNT}}{\varphi} \tag{12}$$

$$\beta_{np} = \frac{\varphi_{Fe_3O_4}\beta_{Fe_3O_4} + \varphi_{MWCNT}\beta_{MWCNT}}{\varphi} \tag{13}$$

$$k_{np} = \frac{\varphi_{Fe_3O_4}k_{Fe_3O_4} + \varphi_{MWCNT}k_{MWCNT}}{\varphi} \tag{14}$$

$$\sigma_{np} = \frac{\varphi_{Fe_3O_4}\sigma_{Fe_3O_4} + \varphi_{MWCNT}\sigma_{MWCNT}}{\varphi} \tag{15}$$

$$Continuity\ \frac{\partial(U)}{\partial X} + \frac{\partial(V)}{\partial Y} = 0 \tag{16}$$

$$\text{Momentum in X direction}: U\frac{\partial U}{\partial X} + V\frac{\partial U}{\partial Y} = -\frac{\partial P}{\partial X} + \frac{(\rho)_{bf}}{(\rho)(1-\phi)^{2.5}}\mathrm{Pr}\left(\frac{\partial^2 U}{\partial X^2} + \frac{\partial^2 U}{\partial Y^2}\right) - \frac{(\rho)_{bf}}{(\rho)(1-\phi)^{2.5}}\frac{\mathrm{Pr}}{Da}U \tag{17}$$

$$\text{Momentum in Y direction}: U\frac{\partial V}{\partial X} + V\frac{\partial V}{\partial Y} = -\frac{\partial P}{\partial Y} + \frac{(\rho)_{bf}}{(\rho)(1-\phi)^{2.5}}\mathrm{Pr}\left(\frac{\partial^2 V}{\partial X^2} + \frac{\partial^2 V}{\partial Y^2}\right) + \frac{(\rho\beta)}{\rho\beta_{bf}}Ra\mathrm{Pr}\theta - \frac{(\rho)_{bf}}{(\rho)(1-\phi)^{2.5}}\frac{\mathrm{Pr}}{Da}V - \frac{(\rho)_{bf}}{(\rho)(1-\phi)^{2.5}}Ha^2\mathrm{Pr}V \tag{18}$$

$$Energy: U\frac{\partial\theta}{\partial X} + V\frac{\partial\theta}{\partial Y} = \frac{\alpha}{\alpha_{bf}}\left[\left(\frac{\partial^2\theta}{\partial X^2} + \frac{\partial^2\theta}{\partial Y^2}\right)\right] \tag{19}$$

3.2. Boundary conditions

The flow pattern through the considered enclosure was represented using streamlines that were predicted using the mathematical model:

$$\frac{\partial^2\psi}{\partial X^2} + \frac{\partial^2\psi}{\partial Y^2} = \frac{\partial U}{\partial Y} - \frac{\partial V}{\partial X}$$

The boundary conditions explored in this research are as follows:

Circular cylinder walls:

$$\theta = 0, U = 0, V = 0$$

Around the Koch snowflake perimeter:

$$\theta = 1, U = 0, V = 0$$

Nu_{loc} and Nu_{avg} near the elliptical hot surface are calculated by the equations:

$$Nu_{loc} = -\frac{k_{eff}}{k_{fl}}\frac{\partial\theta_{po}}{\partial Y}\Big\}_{Y=0} \quad (20)$$

$$Nu_{avg} = \int_0^1 Nu_{loc}dX \quad (21)$$

Finally, FEM was used to address the aforementioned governing equations and boundary conditions. We used the Galerkin weighted residual approach to convert the governing equations into a set of integral mathematical equations.

4. Validation and mesh evaluation

Numerous grids are checked to arrive at the grid independence conclusions. As demonstrated in Table 2, this modeling may be carried out using a grid size of 40060. To ensure the numerical approach used and the approved code is accurate, the flow behavior (displayed by streamlines) and the thermal behavior (displayed by isotherms) are compared to previous numerical results of Sheikholeslami *et al.* [52] and presented in Fig. 2.

The findings shown in Fig. 2 in terms of streamlines and isotherms demonstrate an adequate degree of accuracy. As a consequence, our numerical model can produce reliable results.

5. Results and discussion

In Fig. 3, the impact of increasing the Ra number on the contours of streamlines, isotherms, and isotropic lines for Da = 10^{-2}, Ha = 0 and φ = 0.04 and Ra numbers 10^3-10^6 is presented. The purpose of describing these contours is to investigate the changes in buoyancy force in the cavity on the performance of flow and heat transfer parameters. Increasing the Ra number is possible by changing the temperature between the hot and cold sources. By increasing this parameter, the buoyancy force of the fluid, which is the main movement of circulation, is strengthened. By creating a higher intensity flow in the cavity, it will accelerate, and the temperature distribution will be more uniform in the parts between the hot and cold source, and areas with lower heat transfer will be created only in those parts of the cavity to which the flow does not have direct access. In the surrounding parts, the hot barrier is trapped between the angled sections due to the special structure of the flow barrier, and the temperature distribution in these areas is not uniform and has a higher value. Also, in these areas, due to the indirect movement of the fluid, the flow dissipation is particularly significant at higher Ra numbers. Therefore, the amount of irreversibility around the hot barrier is significant. In high Ra numbers around the cold upper wall, the amount of entropy generation is minimal due to the amplification of the flow velocity and the adhesion of the flow to these surfaces.

In the contours of Fig. 4, the Darcy number changes on the streamlines, isotherms, and isotropic lines are given for Ra = 10^5, Ha = 0, and φ = 0.04. This study compared for Da numbers Da = 10^{-5} to Da = 10^{-2}. In these contours, the flow performance and heat transfer of the studied geometry are compared with the changes in the permeability of the flow cross-section. As the Da number increases, the penetration of the flow cross-section in the cavity increases, and the flow circulates in the cavity with less dissipation due to the buoyancy force. Therefore, the flow intensity is amplified at higher Da numbers, and the mass flow rate is intensified at each cavity section.

On the other hand, heat dissipation improves with increasing Da number, and temperature gradients decrease. The created irreversibility in the cavity is affected by the reduction of the Da number due to the intensification of the hot areas and the decrease of the fluid velocity in the lower Da numbers. By amplifying the Da number, heat will be distributed more evenly between the flow layers and cavity sections.

The contours of Fig. 5 show the effect of increasing the Ha number on the streamlines, isotherms, and isotropic lines for the values of Ra = 10^5, Da = $10^{-2,}$ and φ = 0.04. This study compared Ha numbers Ha = 100 to Ha = 0. In these contours, the studied geometry's flow performance and heat transfer are compared with changes in Lorentz force or Hartmann number. Applying Lorentz force, if not in the flow direction, causes the flow velocity to be depleted and fluid flow in the cavity to be facilitated. Also, if the magnetic field application is not in line with the gravitational force in the cold inner parts, it will cause the fluid to flow slowly from the cold surfaces, which will disturb the uniform temperature distribution. Between the dimensional temperature distribution diagrams, parts such as the surfaces on the hot barrier and the surrounding area will move slowly due to the Lorentz force between the angled surfaces, and the flow rate depreciation is significant; hence; the cavity temperature in these areas, especially the parts around the source will be increased. Due to the lack of uniform temperature distribution and velocity depreciation in the parts around the hot source, the amount of generated entropy has increased.

In the contours of Fig. 6, the position of hot barrier placement on the streamlines, isotherms, and isotropic lines for the values of Ra = 10^5, Da = 10^{-2}, and φ = 0.04 in the state without applying a magnetic field is given. In these contours, the flow and heat transfer performance of the studied geometry is described and plotted with changes in the position of the hot barrier. Placing a hot barrier in different parts of the cavity disturbs the mass balance on both sides of the cavity, especially for the barrier position in the left and right parts, where the behavior is quite apparent. Among the studied cases, placing

Table 2 Nu_{avg} and $|\psi|_{max}$ for various grid resolutions.

grid resolutions	4226	6538	16,422	40,060	47,880
Nu_{avg}	2.4844	2.5929	2.8120	2.9443	2.9446
$\|\psi\|_{max}$	9.7529	9.7648	9.7772	9.7846	9.7857

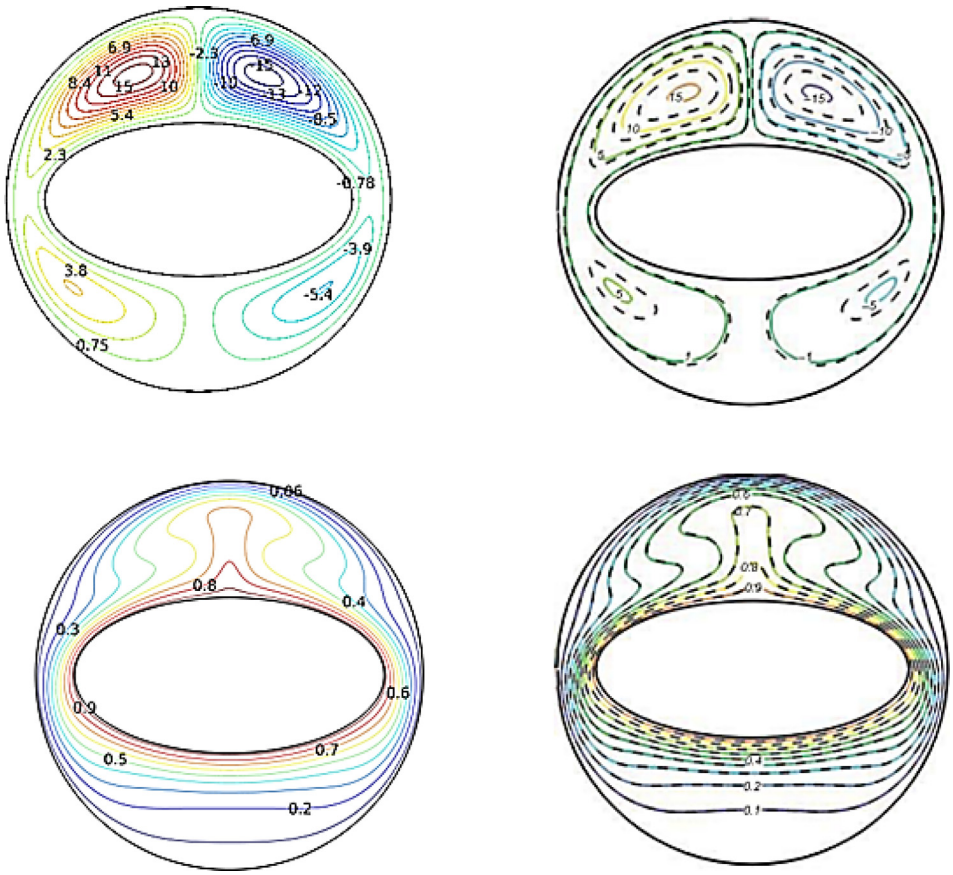

Fig. 2 Streamlines and isotherm contours of the current study [right] and Sheikholeslami et al. [55] [left].

a barrier in the lower part of the cavity can increase the length of the vortex and strengthen the momentum of the circulating fluid in the cavity, but it disrupts the uniform temperature distribution above the barrier. On the other hand, placing a barrier on the left and right sides of the cavity also disturbs the temperature balance in parts of the cavity where the fluid velocity decreases. These areas are obstructed at the top and are quite visible around the central regions of the cavity. Placement of the barrier in the upper part of the cavity due to less access of natural flow to the lower part of the barrier will cause non-uniform distribution and increase irreversibility in these areas.

In the diagrams of Fig. 7, the variations of the average Nusselt number with parameters such as hot barrier location, Ha number, Da number, and nanoparticles concentration are shown in Ra numbers 10^3 to 10^6. Fig. 7a presents the changes in the average Nusselt number affected by different Lorentz force values according to the gravitational acceleration for the Ha number for the Da number 10^{-2}. In these diagrams, the increase in Lorentz force causes substantial changes in the small values of the Nusselt number. In fact, due to the direction of the magnetic force, the Lorentz force is in agreement with the gravitational force. Therefore, in addition to separating the hot flow in the lower part of the barrier, increasing the Lorentz force strengthens the separation of the flow in the upper part of the cold source. All of the above behaviors will eventually reduce the Nusselt number by amplifying the Ha number. At a Ra number less than 10^4, the behavior of Fig. 7 a shows that the natural convection is slow and the heat transfer phenomena are similar to conduction, and increasing the Ha number will not improve heat transfer. With increasing Ra number, due to the importance of flow circulation in the cavity, the application of Lorentz force with different intensities becomes essential. Applying a Lorentz force with a higher Ha number at high Ra numbers reduces heat transfer due to junction balance and flow separation on hot and cold surfaces. The changes in the average Nusselt number versus concentrations are plotted in Fig. 7b. This investigation is performed for the state without applying a magnetic field for Da = 10^{-2}. The presence of solid nanoparticles in memory due to improved thermal conductivity can increase heat transfer.

On the other hand, adding solid nanoparticles to the base liquid can grow the viscosity and cooling fluid compared to the base liquid. In the studied geometry in some parts of the cavity, increasing the above properties in a higher volume fraction can significantly improve the Nusselt number. On the other hand, the above behavior has the opposite behavior for different surfaces, especially surfaces that are not in the direction of direct and strong circulation of liquid. In general, the presence of solid nanoparticles in the diagrams of Fig. 7b has had a limited impact on the growth of the Nusselt number, and this is the case for almost all Ra numbers. The effect of the average Nusselt number behavior with the Da number changes is plotted in the diagrams in Fig. 7c. This investigation was performed for Ha = 50. As the Da number rises, the permeability of the moving surface grows. Reducing the permeability

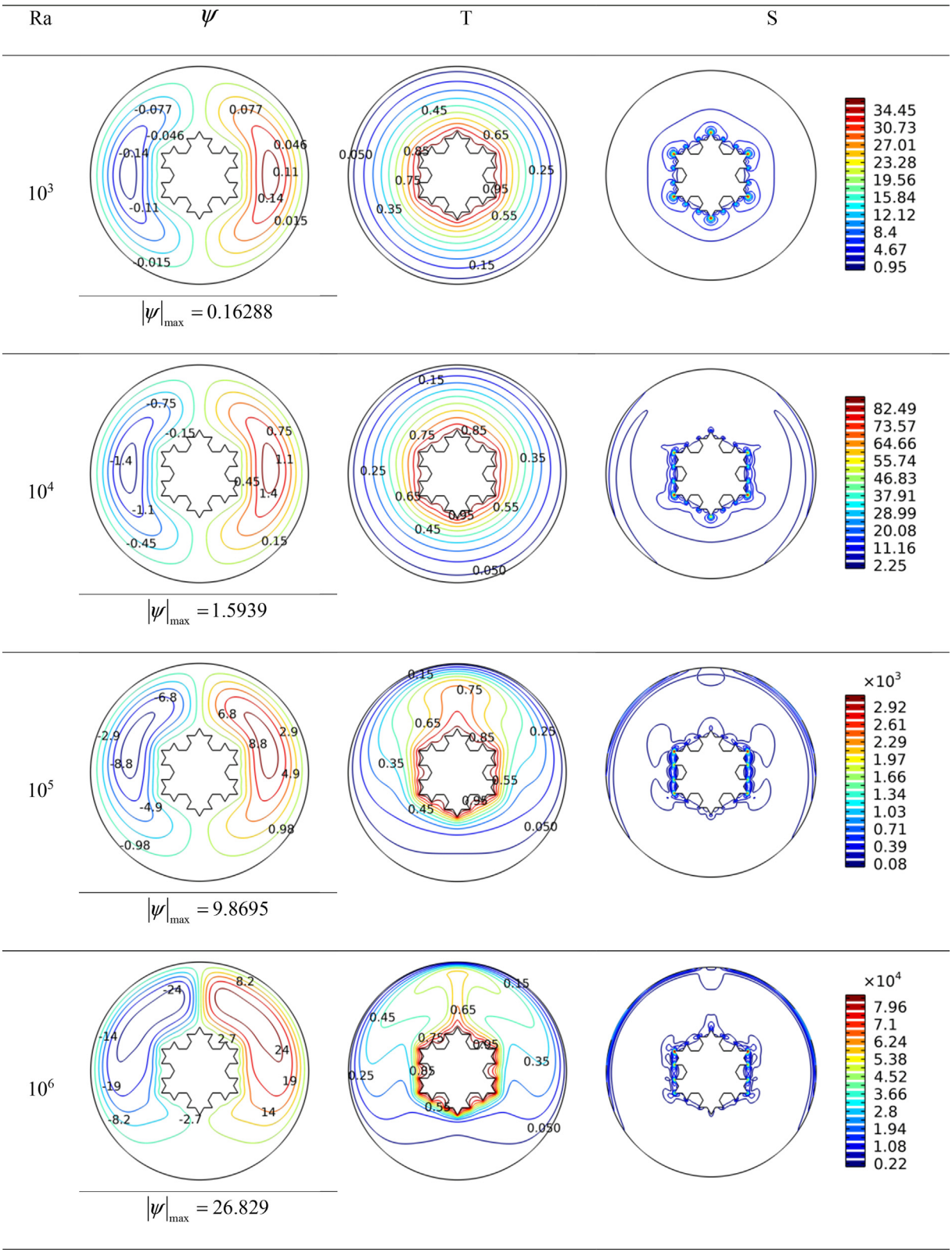

Fig. 3 Ra number influence on streamlines and isotherms for Da = 10^{-2}, Ha = 0.

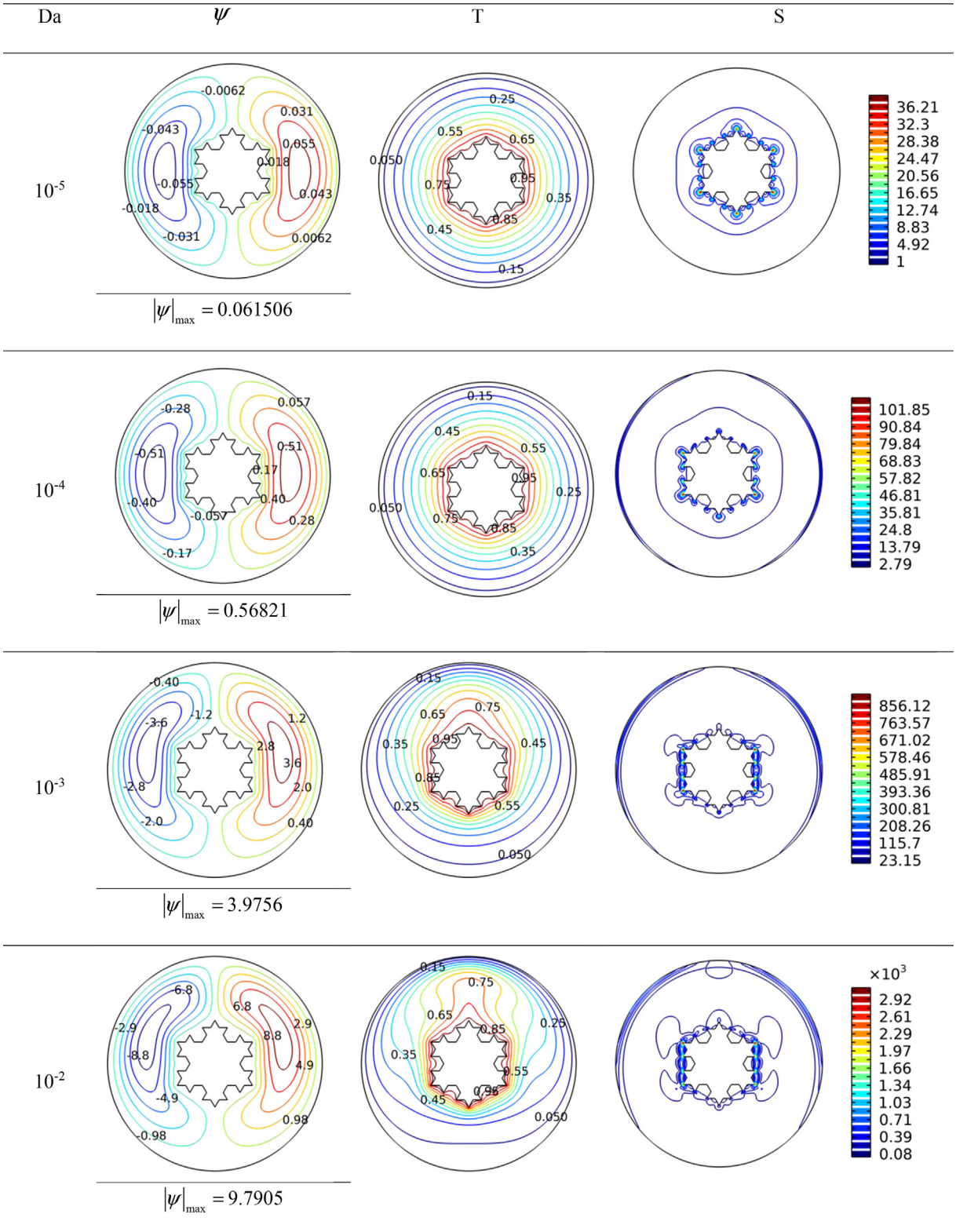

Fig. 4 Da number influence on streamlines and isotherms for Ra = 10^5, Ha = 0, and φ = 0.04.

of the flow cross-section obstructs the fluid circulation path and depletes the fluid movement.

The predominant mechanism of fluid motion in the chamber is with the help of thermosyphon force. The creatures created density change between the hot and cold areas of the cavity, causing the formation of this mechanism. Blockage of the flow by reducing the Da number will weaken the heat transfer rate. This behavior in the diagrams of Fig. 7c has

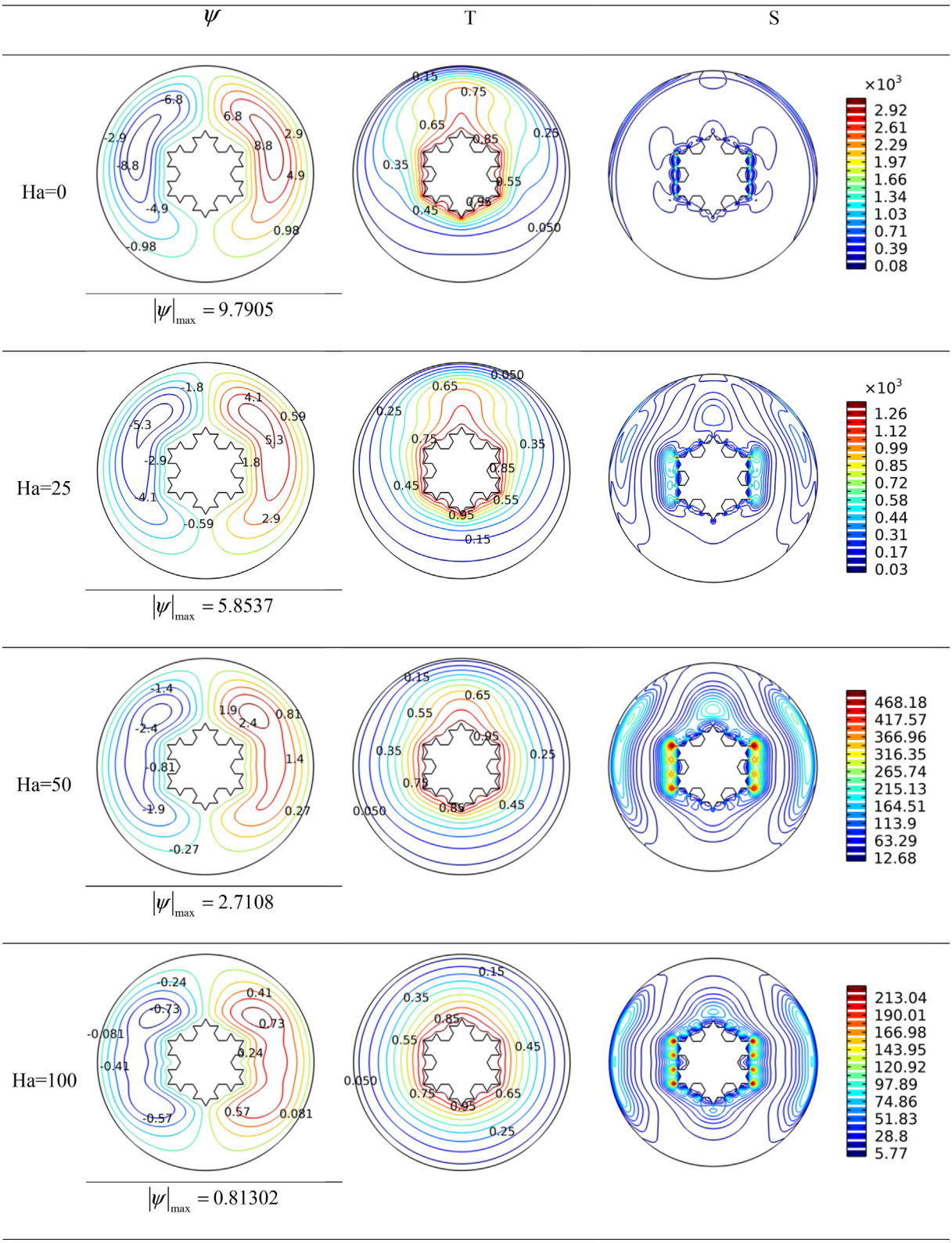

Fig. 5 Ha number influence on streamlines and isotherms for Ra = 10^5, Da = $10^{-2.}$

reduced the Nusselt number. As the permeability decreases, although the Ra number also grows, the Nusselt number decreases due to the weakening and depreciation of the fluid motion components. The changes in Nusselt number behavior by displacing the hot barrier in the cavity for 5 different cases are plotted in the diagrams in Fig. 7d. The position of the hot barrier can strengthen the fluid circulation and prevent the fluid from moving, or it can have the opposite behavior. Plac-

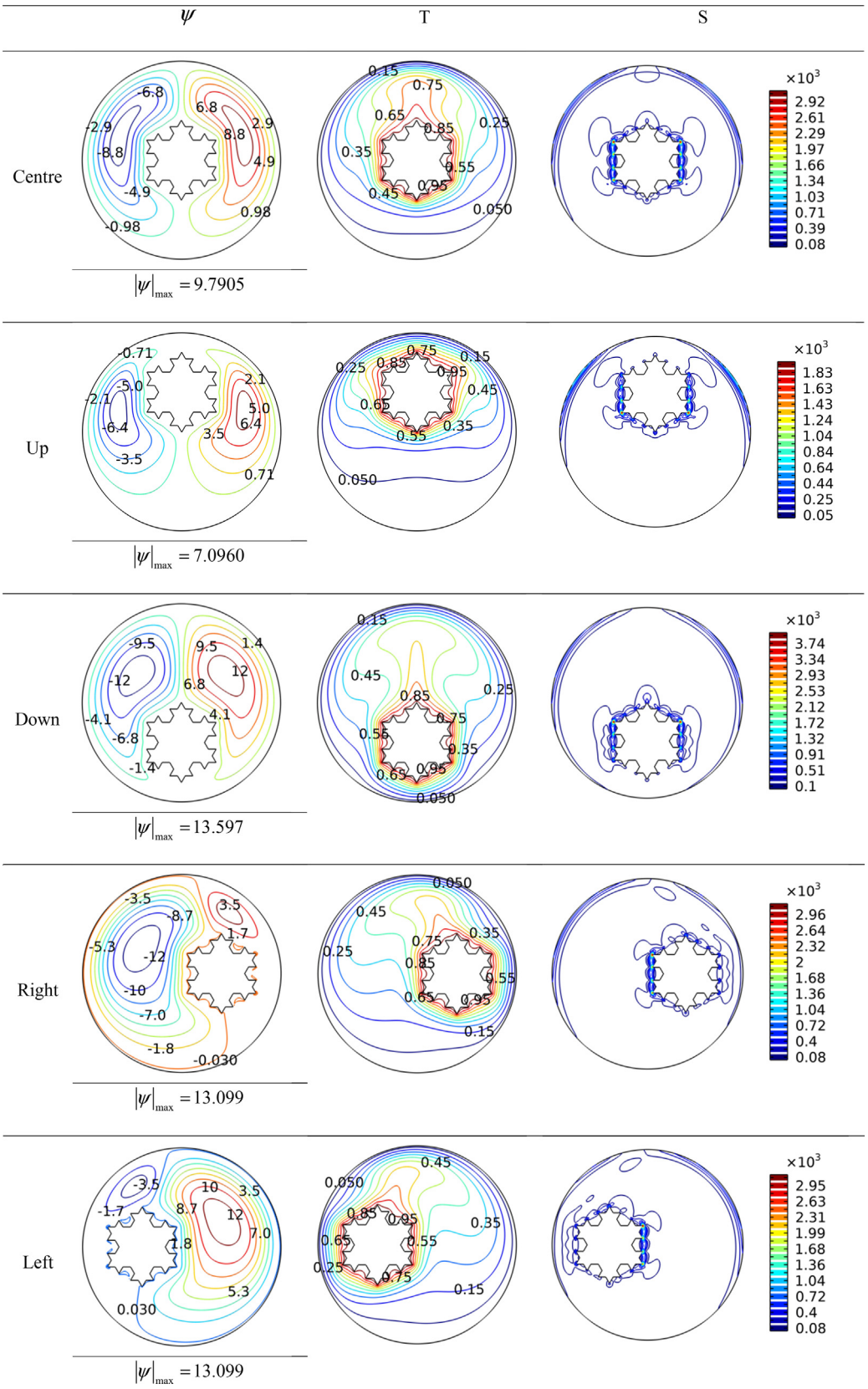

Fig. 6 Koch snowflake's position influence on streamlines and isotherms for Ra = 10^5, Da = 10^{-2}, Ha = 0.

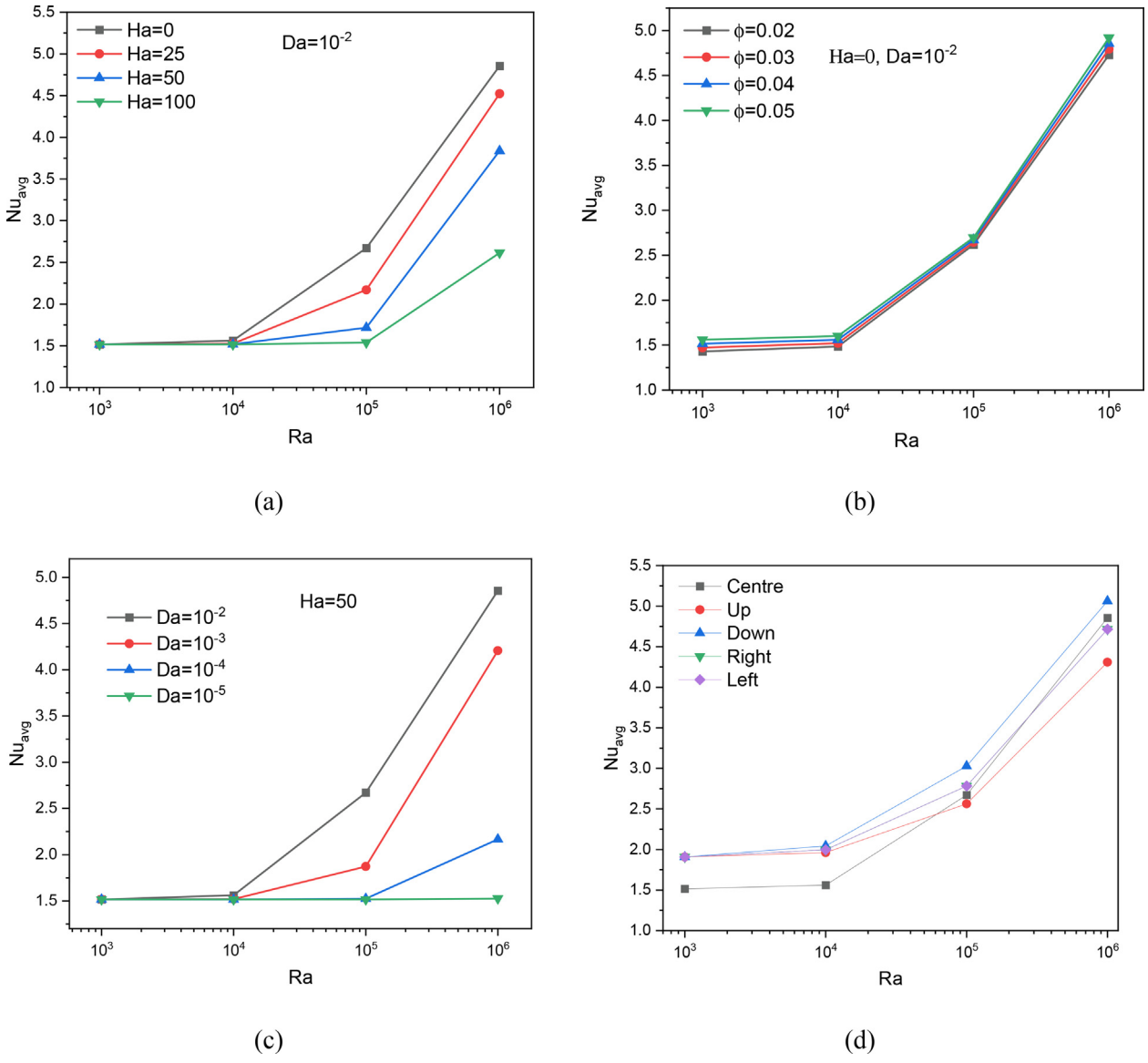

Fig. 7 Nu_{avg} for different parameters.

ing a hot barrier in any area can enhance the vortex with high or low intensity. The variation of the Nusselt number versus the position of the hot barrier in the cavity is limited to Ra numbers less than 10^4. The location of the barrier for both sides of the cavity is the same due to the same boundary conditions and only the change of flow direction. The worst-case scenario for a hot barrier is to install it at the top of the cavity, as a higher-intensity liquid circulation path is not provided, and the distance between the hot and cold source is reduced. Therefore, a hot barrier above the cavity is not recommended for $Ra > 10^4$. The best way to install a heat barrier is at the bottom of the cavity. The cause is due to the increase of the path without hot and cold sources and the strengthening of the intensity of liquid circulation from the place of contact with the hot source to reach the upper of the cavity and the cold source. Placing a hot barrier in Ra numbers less than 10^5 will create the lowest heat transfer rate among the studied conditions. Therefore, it is recommended to use this mode for $Ra > 10^5$.

The variations of the Bejan number in the diagrams of Fig. 8 are plotted at $Ra = 10^3$ to 10^6 with increasing Ha number, Da number, the volumetric fraction of nanoparticles, and hot barrier location. The values of the Bejan number due to the application of different Ha numbers for the $Da = 10^{-2}$ are plotted in Fig. 7a. In these diagrams, the Lorentz force changes have caused dramatic changes in the Bejan number. The range of changes in these diagrams indicates that at low Ra numbers, the Bejan number tends to be 1, indicating a significant increase in temperature gradients in the cavity and the expansion of the thermal boundary layer at low fluid velocities. At low velocities of the fluid, due to the reduction of velocity and motion components in the porous medium, the growth of temperature gradients is a direct result of the increase in thermal conductivity of the moving surface caused by (the fluid–solid cross-sectional combination). For this purpose, a high-conductivity environment is created in which heat penetration increases. Increasing the temperature in the flow section reduces the temperature difference between the fluid

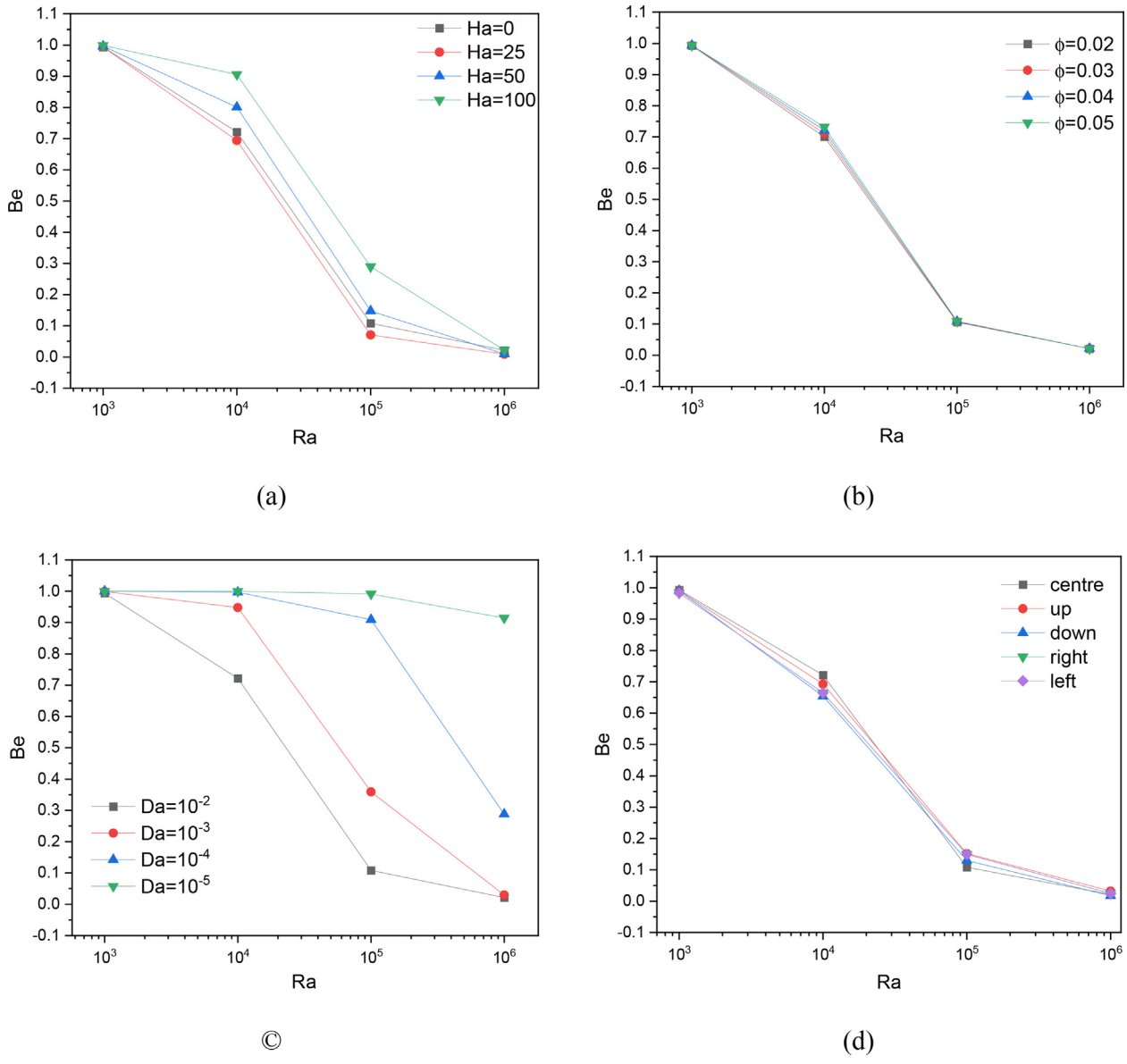

Fig. 8 Bejan number for different parameters.

layers, which will enhance the irreversibility due to the heat transfer. By growing the Ray number and amplifying the flow rate in the chamber, the heat transfer between the hot and cold sources is accelerated. Increasing the Ra number reduces the irreversibility due to lack of heat dissipation and the creation of hot zones, and the behavior of Bejan number diagrams tends to 0. Increasing the Ra number and improving fluid motion, and better heat distribution will increase the friction factor. Increasing the Ha number strengthens the irreversibility and strengthens the Bejan number values. Increasing the Ha number at low Ra numbers will increase fluid stagnation and the temperature gradient.

At higher Ra numbers, high-intensity Lorentz aerosols disrupt fluid movement and increase the friction factor. At Ra number 10^3, due to the low velocity of the fluid, increasing the Ra number will have an effect on the Bejan number changes, and its value depends only on the growth of temperature gradients and is approximately constant. In Ra number 10^6, due to the fluid motion intensification due to the buoyancy force growth, the Bijan number changes are not dependent on the Lorentz force and its intensity, and the Bijan number is a constant value. The behavior of Bejan number values affected by the addition of a volumetric fraction of nanoparticles is plotted in the diagrams in Fig. 7b. This test is plotted for the state without applying a magnetic field for Da = 10^{-2}. Added solid nanoparticles to improve heat transfer can increase viscosity and density. Increased viscosity affects the behavior of the friction factor and increases the irreversibility due to the friction.

On the other hand, improving thermal conductivity eliminates temperature gradients and reduces irreversibility due to non-uniform temperature distribution. Increasing nanoparticle volume fraction will have a limited effect on Bejan number changes. The presence of nanoparticles can neutralize changes in the Bejan number at different volume fractions, and the trend of the graphs is almost constant. The effectiveness of

Bejan number behavior with the changes in the penetration of the flow cross-section in the cavity (Da number) is plotted in the diagrams in Fig. 7c. This test was performed for Ha = 50. The presence of a porous medium in a cavity with different penetration can strongly affect the movement of the fluid, and there are significant changes in the depreciation of the flow velocity. Decreasing the Da number is associated with reducing the flow's cross-sectional area and obstructing the fluid's movement. As the Da number decreases, the permeability decreases, and changes in temperature gradients and gradients increase.

On the other hand, by decreasing the Da number, the porosity level in the cavity increases, and the heat penetration also increases. Changes in the Bejan number by moving the hot barrier in the cavity for five different cases are plotted in the diagrams in Fig. 7d. The presence of a hot barrier in the cavity due to disruption of the natural circulation of the fluid can cause limited changes in the Bejan number. On the other hand, because the upper, lower, left, and right areas of the thermal barrier are also involved in the formation of the circulatory system, most variations of the Bejan number were reported for Ra 10^4 and 10^5. In summary, Da number reduction compared to the Ha number growth, the volume fraction, and changes in cavity position can intensify the growth of temperature gradients and the resulting irreversibility.

6. Conclusion

The present work examined the natural and laminar motion of Fe_3O_4-MWCNT/water hybrid nanofluid in a volumetric fraction of 0–5 %. This study aimed to investigate the influence of temporary changes in hot barrier location, application of magnetic force, and an increase of Ra and Da numbers on natural convection of porous annulus cavity between the cylinder and Koch snowflake. The findings of the present study can be summarized in the following points:

- For a higher intensity flow in the chamber, the heat transfer will be accelerated, and the temperature distribution will be more uniform in the parts between hot and cold sources.
- Due to the shape of the barrier, the flow is trapped between the angled sections, and the temperature distribution in these areas is not uniform and has a higher value.
- The created irreversibility in the cavity, as shown by Bejan number, is affected by the reduction of the Da number due to the intensification of the hot areas and the decrease of the fluid velocity.
- By increasing the Da number, heat will be distributed more evenly between the flow layers and in the cavity sections.
- As expected, the presence of solid nanoparticles improves thermal conductivity and hence improves heat transfer.
- At the highest Ra, increasing Ha from 0 to 100 decreased Nuavg by 50 %.
- Placing the hot barrier at the bottom of the chamber results in the highest Nu_{avg} compared to other barrier positions.
- By increasing the Ra number and amplifying the flow rate in the cavity, the heat transfer between the hot and cold sources is accelerated.
- Increasing the Ra number reduces the irreversibility due to lack of heat dissipation and the creation of hot zones, and the Bejan number tends to 0.
- As the Da number decreases, the permeability decreases, and changes in temperature gradients and gradients increase.
- It was found that, at the highest, Ra, decreasing Da from 10^{-2} to 10^{-5} reduced Nuavg by 70 %.
- For the above reasons, the better the flow surface permeability, the less obstruction the fluid moves, and the less irreversible effects of its temperature gradients.

Declaration of Competing Interest

The authors declare that they have no known competing financial interests or personal relationships that could have appeared to influence the work reported in this paper.

Acknowledgments

The authors extend their appreciation to the Deanship of Scientific Research at King Khalid University for funding this work through Research Group Project under grant number (RGP.1/322/43). The authors would like to thank the Deanship of Scientific Research at Umm Al-Qura University for supporting this work by Grant Code: (22UQU4331317DSR89).

References

[1] S.U.S. Choi, Enhancing thermal conductivity of fluids with nanoparticles, Am. Soc. Mech. Eng. Fluids Eng. Div. FED 231 (January 1995) (1995) 99–105.
[2] X. Zhang, F. Ma, S. Yin, C.D. Wallace, M.R. Soltanian, Z. Dai, X. Lü, Application of upscaling methods for fluid flow and mass transport in multi-scale heterogeneous media: A critical review, Appl. Energy 303 (2021) 117603, https://doi.org/10.1016/j.apenergy.2021.117603.
[3] B. Bai, D. Rao, T. Chang, Z. Guo, A nonlinear attachment-detachment model with adsorption hysteresis for suspension-colloidal transport in porous media. J. Hydrol. 578 (2019) 124080. https://doi.org/10.1016/j.jhydrol.2019.124080
[4] B. Bai, Y. Wang, D. Rao, F. Bai, The Effective Thermal Conductivity of Unsaturated Porous Media Deduced by Pore-Scale SPH Simulation, Front. Earth Sci. (2022), https://doi.org/10.3389/feart.2022.943853.
[5] L. Tang, Y. Zhang, C. Li, Z. Zhou, X. Nie, Y. Chen, H. Cao, et al., Biological stability of water-based cutting fluids: progress and application. Chin. J. Mech. Eng., 35(1) (2022)1-24. https://doi.org/10.1186/s10033-021-00667-z.
[6] D. Jia, Y. Zhang, C. Li, M. Yang, T. Gao, Z. Said, et al, Lubrication-enhanced mechanisms of titanium alloy grinding using lecithin biolubricant, Tribol Int. 169 (2022) 107461, https://doi.org/10.1016/j.triboint.2022.107461.
[7] A.S. Rikani, Investigation of turbulent fluid flow in the presence of a magnetic field induced dynamic motion of the vessel, J. Res. Sci. 9 (01) (2021) 74–94.
[8] A.B.W. PUTRA, Computer Technology Simulation towards Power Generation Potential from Coproduced Fluids in South Lokichar Oil Fields, Int. J. Commun. Comput. Technol. 8 (2) (2020) 9–12, https://doi.org/10.31838/ijccts/08.02.03.
[9] G. Zhang, J. Chen, Z. Zhang, M. Sun, Y. Yu, J. Wang, S. Cai, Analysis of magnetorheological clutch with double cup-shaped gap excited by Halbach array based on finite element method and experiment, Smart Mater. Struct. 31 (7) (2022) 075008, https://doi.org/10.1088/1361-665X/ac701a.

[10] M. Yang, C. Li, Y. Zhang, D. Jia, X. Zhang, Y. Hou, et al, Maximum undeformed equivalent chip thickness for ductile-brittle transition of zirconia ceramics under different lubrication conditions, Int. J. Mach. Tools Manuf. 122 (2017) 55–65, https://doi.org/10.1016/j.ijmachtools.2017.06.003.
[11] M. Ghobadi, Based on copper ferrite nanoparticles (CuFe2O4 NPs): Catalysis in synthesis of heterocycles, J. Synth. Chem. 1 (2022) 84–96, https://doi.org/10.22034/jsc.2022.155234.
[12] Y. Wang, C. Li, Y. Zhang, M. Yang, B. Li, L. Dong, J. Wang, Processing characteristics of vegetable oil-based nanofluid MQL for grinding different workpiece materials, International Journal of Precision Engineering and Manufacturing-Green Technology 5 (2) (2018) 327–339. https://doi.org/10.1007/s40684-018-0035-4.
[13] A. Bilal, F. Mabood, Numerical Investigation of Mixed Convection Flow of Viscoelastic Nanofluid with Convective Conditions over an Exponentially Stretching Surface, Iran. J. Chem. Chem. Eng. 40 (6) (2021) 1931–1942.
[14] S. Asleshirin, H. Mazaheri, M. Omidkhah, A. Hassani Joshaghani, Investigation of Thermophysical Properties of Io Nanofluids Containing Multi-Walled Carbon Nanotubes and Graphene, Iranian Journal of Chemistry and Chemical Engineering (IJCCE) 41 (2) (2022) 380–391, https://doi.org/10.30492/ijcce.2020.121326.4273.
[15] R. Zahmatkesh, H. Mohammadiun, M. Mohammadiun, M. Dibaei Bonab, M. Sadi, Theoretical Investigation of Entropy Generation in Axisymmetric Stagnation Point Flow of Nanofluid Impinging on the Cylinder Axes with Constant Wall Heat Flux and Uniform Transpiration, Iran, J. Chem. Chem. Eng. 40 (6) (2021) 1893–1908, https://doi.org/10.30492/ijcce.2020.43346.
[16] J. Zhang, C. Li, Y. Zhang, M. Yang, D. Jia, G. Liu, Y. Hou, R. Li, N. Zhang, Q. Wu, H. Cao, Experimental assessment of an environmentally friendly grinding process using nanofluid minimum quantity lubrication with cryogenic air, Journal of cleaner production 193 (2018) 236–248. https://doi.org/10.1016/j.jclepro.2018.05.009.
[17] A. M. Aly, E. M. Mohamed, and N. Alsedais, "Double-diffusive convection from a rotating rectangle in a finned cavity filled by a nanofluid and affected by a magnetic field," *Int. Commun. Heat Mass Transf.*, vol. 126, no. May, 2021, doi: 10.1016/j.icheatmasstransfer.2021.105363.
[18] W. T. Wu, M. Massoudi, and H. Yan, "Heat transfer & flow of nanofluids in a Y-Type intersection channel with multiple pulsations: A numerical study," *Energies*, vol. 10, no. 4, 2017, doi: 10.3390/en10040492.
[19] S. Hussain, M. Jamal, B.P. Geridonmez, Impact of fins and inclined magnetic field in double lid-driven cavity with Cu–water nanofluid, Int. J. Therm. Sci. 161 (August) (2020) 2021, https://doi.org/10.1016/j.ijthermalsci.2020.106707.
[20] G. Zhang, Z. Zhang, M. Sun, Y. Yu, J. Wang, S. Cai, The Influence of the Temperature on the Dynamic Behaviors of Magnetorheological Gel, Adv. Eng. Mater. 2101680 (2022), https://doi.org/10.1002/adem.202101680.
[21] B.J. Gireesha, G. Sowmya, M.I. Khan, H.F. Öztop, Flow of hybrid nanofluid across a permeable longitudinal moving fin along with thermal radiation and natural convection, Comput. Methods Programs Biomed. 185 (2020), https://doi.org/10.1016/j.cmpb.2019.105166.
[22] S. Hejri and E. H. Malekshah, "Cooling of an electronic processor based on numerical analysis on natural convection and entropy generation over a dissipating fin equipped with copper oxide/water nanofluid with Koo-Kleinstreuer-Li model," *Therm. Sci. Eng. Prog.*, vol. 23, no. March, 2021, doi: 10.1016/j.tsep.2021.100916.
[23] M. Gholami, M.R. Nazari, M.H. Talebi, F. Pourfattah, O.A. Akbari, D. Toghraie, Natural convection heat transfer enhancement of different nanofluids by adding dimple fins on a vertical channel wall, Chinese J. Chem. Eng. 28 (3) (Mar. 2020) 643–659, https://doi.org/10.1016/j.cjche.2019.11.001.
[24] M. Sheremet, Ioan Pop, Natural Convection in a Wavy Porous Cavity With Sinusoidal Temperature Distributions on Both Side Walls Filled With a Nanofluid: Buongiorno's Mathematical Model, Transport in Porous Media, Transp Porous Med 105 (2014) 411–429, https://doi.org/10.1007/s11242-014-0375-7.
[25] Shu-Rong Yan, Ahmad Hajatzadeh Pordanjani, Saeed Aghakhani, Aysan Shahsavar Goldanlou, Masoud Afrand, Managment of natural convection of nanofluids inside a square enclosure by different nano powder shapes in presence of Fins with different shapes and magnetic field effect, Advanced Powder Technology, 31(7),2020, 2759-2777.
[26] M. Siavashi, R. Yousofvand, S. Rezanejad, Nanofluid and porous fins effect on natural convection and entropy generation of flow inside a cavity, Adv. Powder Technol. 29 (1) (2018) 142–156, https://doi.org/10.1016/j.apt.2017.10.021.
[27] K. Al-Farhany, K.K. Al-Chlaihawi, M.F. Al-dawody, N. Biswas, A.J. Chamkha, Effects of fins on magnetohydrodynamic conjugate natural convection in a nanofluid-saturated porous inclined enclosure, Int. Commun. Heat Mass Transf. 126 (2021), https://doi.org/10.1016/j.icheatmasstransfer.2021.105413 105413.
[28] A. Abdulkadhim et al, Effect of heat generation and heat absorption on natural convection of Cu-water nanofluid in a wavy enclosure under magnetic field, Int. Commun. Heat Mass Transf. 120 (November 2021) (2020), https://doi.org/10.1016/j.icheatmasstransfer.2020.105024.
[29] A. Abdulkadhim, I.M. Abed, N.M. Said, Magnetohydrodynamics thermogravitational convective in a novel I-shaped wavy-walled enclosure considering various inner hot pipe locations, J. Therm. Anal. Calorim. (Sep. 2021), https://doi.org/10.1007/s10973-021-11072-y.
[30] S.M. Seyyedi, M. Dayyan, S. Soleimani, E. Ghasemi, Natural convection heat transfer under constant heat flux wall in a nanofluid filled annulus enclosure, Ain Shams Eng. J. 6 (1) (2015) 267–280, https://doi.org/10.1016/j.asej.2014.09.003.
[31] T. Tayebi, A.J. Chamkha, A.A. Melaibari, E. Raouache, Effect of internal heat generation or absorption on conjugate thermal-free convection of a suspension of hybrid nanofluid in a partitioned circular annulus, Int. Commun. Heat Mass Transf. vol. 126, no. June (2021), https://doi.org/10.1016/j.icheatmasstransfer.2021.105397 105397.
[32] Y.P. Hu, Y.R. Li, L. Lu, Y.J. Mao, M.H. Li, Natural convection of water-based nanofluids near the density maximum in an annulus, Int. J. Therm. Sci. 152 (August 2019) (2020) 106309, https://doi.org/10.1016/j.ijthermalsci.2020.106309.
[33] P. Gholamalipour, M. Siavashi, M.H. Doranehgard, Eccentricity effects of heat source inside a porous annulus on the natural convection heat transfer and entropy generation of Cu-water nanofluid, Int. Commun. Heat Mass Transf. 109 (November) (2019), https://doi.org/10.1016/j.icheatmasstransfer.2019.104367 104367.
[34] J. Belabid, K. Allali, Thermo-bioconvection in horizontal wavy-walled porous annulus, Eur. J. Mech. B/Fluids 89 (2021) 421–429, https://doi.org/10.1016/j.euromechflu.2021.07.006.
[35] F.S. Oğlakkaya, C. Bozkaya, MHD natural convection in a semi-annulus enclosure filled with water-based nanofluid using DRBEM, Eng. Anal. Bound. Elem. 71 (Oct. 2016) 151–163, https://doi.org/10.1016/j.enganabound.2016.07.013.
[36] H. Guan, S. Huang, J. Ding, F. Tian, Q. Xu, J. Zhao, Chemical environment and magnetic moment effects on point defect formations in CoCrNi-based concentrated solid-solution alloys, Acta Mater. 187 (2020) 122–134, https://doi.org/10.1016/j.actamat.2020.01.044.
[37] S.Y. Motlagh, E. Golab, A.N. Sadr, Two-phase modeling of the free convection of nanofluid inside the inclined porous semi-

annulus enclosure, Int. J. Mech. Sci. 164 (August) (2019), https://doi.org/10.1016/j.ijmecsci.2019.105183 105183.

[38] M. Hatami, J. Zhou, J. Geng, D. Jing, Variable magnetic field (VMF) effect on the heat transfer of a half-annulus cavity filled by Fe3O4-water nanofluid under constant heat flux, J. Magn. Magn. Mater. 451 (2018) 173–182, https://doi.org/10.1016/j.jmmm.2017.10.110.

[39] S. Munawar, N. Saleem, W.A. Khan, ''Entropy generation minimization E.G.M. analysis of free convective hybrid nanofluid flow in a corrugated triangular annulus with a central triangular heater,'' *Chinese*, J. Phys. (2021), https://doi.org/10.1016/j.cjph.2021.10.028.

[40] A. Miles, R. Bessaïh, Heat transfer and entropy generation analysis of three-dimensional nanofluids flow in a cylindrical annulus filled with porous media, Int. Commun. Heat Mass Transf. 124 (2021), https://doi.org/10.1016/j.icheatmasstransfer.2021.105240 105240.

[41] A.S. Dogonchi, Hashim, Heat transfer by natural convection of Fe3O4-water nanofluid in an annulus between a wavy circular cylinder and a rhombus, Int. J. Heat Mass Transf. 130 (2019) 320–332, https://doi.org/10.1016/j.ijheatmasstransfer.2018.10.086.

[42] A. Bouzerzour, M. Djezzar, H.F. Oztop, T. Tayebi, N. Abu-Hamdeh, Natural convection in nanofluid filled and partially heated annulus: Effect of different arrangements of heaters, Phys. A Stat. Mech. its Appl. 538 (2020), https://doi.org/10.1016/j.physa.2019.122479 122479.

[43] M. Sheikholeslami, M. Gorji-Bandpy, D.D. Ganji, Numerical investigation of MHD effects on Al2O3-water nanofluid flow and heat transfer in a semi-annulus enclosure using LBM, Energy 60 (2013) 501–510, https://doi.org/10.1016/j.energy.2013.07.070.

[44] F. Berrahil, A. Filali, C. Abid, S. Benissaad, R. Bessaih, O. Matar, Numerical investigation on natural convection of Al2O3/water nanofluid with variable properties in an annular enclosure under magnetic field, Int. Commun. Heat Mass Transf. vol. 126, no. July (2021), https://doi.org/10.1016/j.icheatmasstransfer.2021.105408 105408.

[45] E. D. Aboud *et al.*, ''MHD effect on mixed convection of annulus circular enclosure filled with Non-Newtonian nanofluid,'' *Heliyon*, vol. 6, no. 4, 2020, doi: 10.1016/j.heliyon.2020.e03773.

[46] T. Tayebi, A. Sattar Dogonchi, N. Karimi, H. Ge-JiLe, A.J. Chamkha, Y. Elmasry, Thermo-economic and entropy generation analyses of magnetic natural convective flow in a nanofluid-filled annular enclosure fitted with fins, Sustain. Energy Technol. Assessments 46 (May) (2021), https://doi.org/10.1016/j.seta.2021.101274 101274.

[47] A. Shahsavar, M. Jafari, I.B. Askari, F. Selimefendigil, Thermo-hydraulic performance and entropy generation of biologically synthesized silver/water-ethylene glycol nano-fluid flow inside a rifled tube using two-phase mixture model, Energy Sources, Part A: Recovery, Utilization, and Environmental Effects (2020), https://doi.org/10.1080/15567036.2020.1850932.

[48] L. Durlofsky, J.F. Brady, Analysis of the Brinkman equation as a model for flow in porous media, Phys. Fluids 30 (11) (1987) 3329, https://doi.org/10.1063/1.866465.

[49] ARABAN, Hadi Pourziaei, ALINEJAD, Javad, et PEIRAVI, Mohammad Mohsen. Entropy generation and hybrid fluid-solid-fluid heat transfer in 3D multi-floors enclosure. International Journal of Exergy, 2022, vol. 37, no 3, p. 337-357.

[50] SEADAWY, Aly R., KUMAR, Dipankar, et CHAKRABARTY, Anuz Kumar. Dispersive optical soliton solutions for the hyperbolic and cubic-quintic nonlinear Schrödinger equations via the extended sinh-Gordon equation expansion method. The European Physical Journal Plus, 2018, vol. 133, no 5, p. 182.

[51] YOUNAS, U., YOUNIS, M., SEADAWY, Aly R., et al. Diverse exact solutions for modified nonlinear Schrödinger equation with conformable fractional derivative. Results in Physics, 2021, vol. 20, p. 103766.

[52] BENDRER, B. A. I., ABDERRAHMANE, Aissa, AHMED, Sameh E., et al. 3D magnetic buoyancy-driven flow of hybrid nanofluids confined wavy cubic enclosures including multi-layers and heated obstacle. International Communications in Heat and Mass Transfer, 2021, vol. 126, p. 105431.

[53] Wasim Jamshed, Mohamed R. Eid, Syed M. Hussain, et al., Physical specifications of MHD mixed convective of Ostwald-de Waele nanofluids in a vented-cavity with inner elliptic cylinder, Int. Commun. Heat Mass Transfer 134 (2022) p. 106038.

[54] Wael Al-Kouz, Abderrahmane Aissa, Aimad Koulali, et al., MHD darcy-forchheimer nanofluid flow and entropy optimization in an odd-shaped enclosure filled with a (MWCNT-Fe3O4/water) using galerkin finite element analysis, Sci. Reports 11(1) (2021) 1–15.

[55] M. Sheikholeslami, CuO-water nanofluid free convection in a porous cavity considering Darcy law, Eur. Phys. J. Plus 132 (1) (Jan. 2017) 55, https://doi.org/10.1140/epjp/i2017-11330-3.